Study of SEPIC and Ćuk Converters Working as Automatic Power Factor Corrector when Operating in Unusual Discontinuous Conduction Modes

Duberney Murillo-Yarce*, Juan Rodriguez, Felipe Loose, Marta Hernando and Javier Sebastian
Universidad de Oviedo, Campus Universitario de Viesques 33204, Gijón, Spain
murilloduberney@uniovi.es*

***Abstract*—It is very well known that the SEPIC and Ćuk converters can operate as Automatic Power Factor Correctors (APFCs) when the converter diode stops conducting during the transistor OFF-state interval, thus achieving operation in the well-known Discontinuous Conduction Mode (DCM). In order to reduce de APFC size, the input inductance can be reduced. However, if that inductance is not high enough, not only the converter diode can stop conducting during the transistor OFF-state interval, but also the input rectifier diodes. Considering the number of diodes that can stop conducting, the aforementioned scenario leads to three DCMs and, consequently, the operation as APFC is not guaranteed anymore. In this paper, the line current waveform of SEPIC and Ćuk converters operating in any of the three aforementioned DCMs is studied in order to evaluate their operation as APFC. The results show that even in the unusual DCMs, the converters operate as quasi-ideal APFCs, thus allowing the design of these converters with lower value of the input inductance and, consequently, with higher power density. The analysis is validated with simulation and experimental results.**

***Index Terms*—multiple discontinuous conduction modes, power factor corrector, SEPIC and Ćuk converters.**

I. Introduction

The use of DC-DC converters operating as Resistor Emulators (RE) plays a crucial role in power factor correction. The behavior of a DC-DC converter as an ER can be achieved by operating the converter in Discontinuous Conduction Mode (DCM) while maintaining a constant duty cycle through the line period [1]. This mode of operation leads to Automatic Power Factor Correctors (APFCs). The study of DCM operation in DC-DC conversion has been extensively addressed in single-switch, single-diode converters, where only one DCM is possible [2]–[4]. However, in cases where multiple diodes belong to different inductive paths, multiple DCMs are possible [5], [6]. An example of multiple DCMs is illustrated by the modified SEPIC converter shown in Fig. 1, where an additional diode is placed at the input port. This modified version of the SEPIC converter can operate in the well-known CCM or in any of three possible DCMs.

When the SEPIC converter works as an ER in an APFC circuit, as depicted in Fig. 2, the input voltage of the converter is not constant, but it varies with the line angle. The input bridge rectifies the line voltage, and its unidirectional current conduction effect can be modeled by introducing a diode in

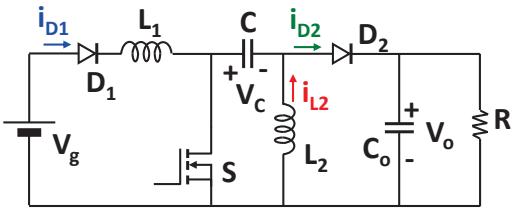

Fig. 1. Modified SEPIC converter with an additional diode at the input port.

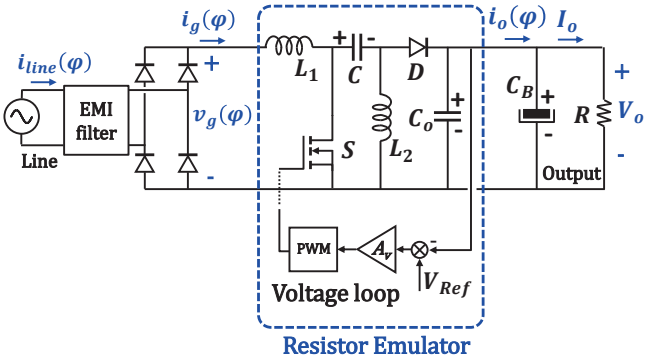

Fig. 2. SEPIC converter operating as an APFC.

series with inductor L_1 as shown in Fig. 1. Consequently, when the SEPIC converter operates in an APFC application, the converter can operate in one or multiple DCMs, depending on the line angle. A well-known scenario is when a pair of the line rectifier diodes remains conducting during each half-period of the line voltage, whereas the SEPIC diode stops conducting during the transistor OFF state. In this DCM (called DCM1 in this paper), the converter inherently acts as an RE, i.e., the line current exhibits the same waveform as the line voltage. Furthermore, the SEPIC can operate in other DCMs (called DCM2 and DCM3 in this paper), or even can change the DCM when the line angle changes. The resulting line current waveform when the converter operates in different DCMs during a line half-period is not known so far.

The results presented in [5] demonstrate that a Ćuk converter with an additional diode at the input port exhibits the

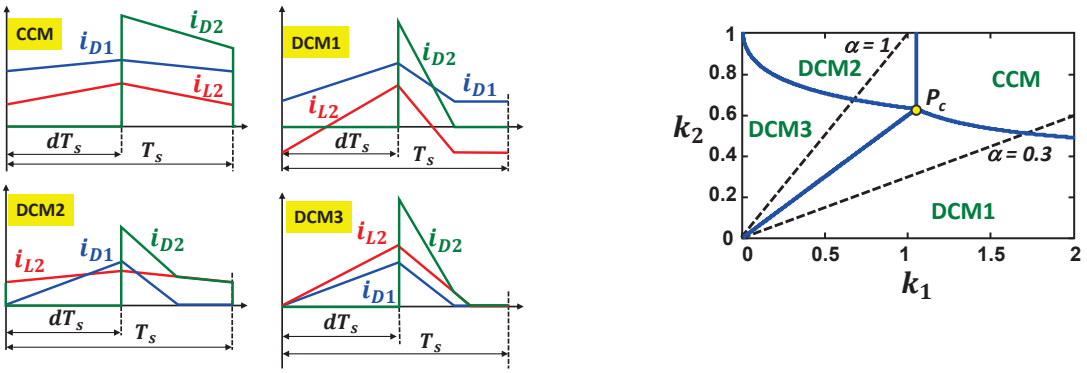

(a) (b)

Fig. 3. Conduction modes corresponding to the modified SEPIC converter shown in Fig. 1: a) Current waveforms through the diodes and inductor L_2. b) Map of conduction regions when $M = 0.6$ and trajectories with $\alpha = 1$ and $\alpha = 0.3$.

same multiple DCMs as the SEPIC converter depicted in Fig. 1. Consequently, the conclusions drawn for the modified SEPIC can be extended to the modified Ćuk as well.

This paper studies the input current waveform of both the SEPIC and Ćuk converters when operating in one or several of these DCMs and working as APFC. The structure of this paper is as follows. The analysis of the conduction modes corresponding to the SEPIC and Ćuk converters with an additional diode at their input port is presented in Section II. This analysis is split into two parts, one devoted to the case of having a constant voltage at the input port (Fig. 1) and the other focused on the case of having a full-wave rectified sinusoidal voltage at the input port (Fig. 2), maintaining the duty cycle constant in each line period. A method to determine the line current waveform in this last case when the converters have been designed to operate in one or in several DCMs is presented in Section III, thus allowing the evaluation of the use of these converters as RE. Section IV shows the simulated and experimental results obtained to validate the prediction of the line current waveform. Finally, Section V presents the conclusions.

II. Analysis of the Conduction Modes in the SEPIC and Ćuk Converters with an Additional Diode

A. Case of Constant Input Voltage

A detailed study of the topology shown in Fig. 1 has been presented in [5]. The most significant current waveforms of the possible conduction modes (one CCM and three DCMs) are shown in Fig. 3(a). Additionally, a plane based on the dimensionless parameters k_1 and k_2 has been built to study these conduction modes [6]. This plane is shown in Fig. 3(b) for closed-loop operation. Each of the parameters k_1 and k_2 is a function of the inductor values L_1 and L_2, as follows:

$$k_1 = \frac{2L_1}{RT_s}, \quad k_2 = \frac{2L_2}{RT_s}, \tag{1}$$

where R is the load resistance and T_s is the switching period. Let us call M the DC conversion ratio defined as $M = V_o/V_g$.

According to [5] and [6], the converter operating point always describes a straight line trajectory in the k_1k_2 plane, due to the synchronous variation of these parameters when load R changes. This trajectory is defined by slope $\alpha = k_2/k_1$. Slope α can be rewritten as $\alpha = L_2/L_1$ using (1). The central point (P_c) of the k_1k_2 plane determines two types of possible trajectories, as Fig. 3(b) shows. According to trajectory slope α and the boundary DCM1-DCM3 (which is a straight line of slope M), two possible design cases can be addressed: (i) $\alpha < M$, which leads to the classical operation involving only the CCM and the DCM1 (which is the well-known DCM); (ii) $\alpha > M$, which leads to the unusual operation involving the CCM, the DCM2 and the DCM3.

All the mathematical expressions that define the multiple DCMs of SEPIC and Ćuk can be found in [5]. The coordinates of P_c are expressed in (2). Equations (3)-(7) show the functions that determine the voltage conversion ratios, whereas (8)-(11) describe the boundaries between modes. Regarding the notation, the subscript 0 refers to the CCM, while subscripts 1, 2 and 3 correspond to the DCMs.

$$k_{1\_P_C}(M) = \frac{1}{M(M+1)}, \quad k_{2\_P_C}(M) = \frac{1}{M+1}, \tag{2}$$

$$M_0(d) = \frac{d}{1-d}, \tag{3}$$

$$M_1(d, k_1, k_2) = \frac{d}{\sqrt{\frac{k_1 k_2}{k_1 + k_2}}}, \tag{4}$$

$$M_2(d, k_1) = \frac{k_1 + \sqrt{k_1(4 + k_1)}}{2k_1} d, \tag{5}$$

$$M_3(d, k_1, k_2) = \frac{A + \sqrt{A^2 + \frac{16k_2^2}{k_1}}}{4k_2} d, \tag{6}$$

$$A = -d + \sqrt{d^2 + 4k_2}. \tag{7}$$

$$F_{0-1}(M,k_1,k_2) = k_2 - \frac{k_1}{(1+M)^2-1} = 0, \quad (8)$$

valid only for $k_1 > k_{1\_P_c}$.

$$F_{0-2}(M,k_1) = k_1 - \frac{1}{M(M+1)} = 0, \quad (9)$$

only valid when $k_2 > k_{2\_P_c}$.

$$F_{1-3}(M,k_1,k_2) = k_2 - Mk_1 = 0, \quad (10)$$

valid only for values verifying $0 < k_1 < k_{1\_P_c}$.

$$F_{2-3}(M,k_1,k_2) = k_2 - 1 + \frac{-k_1 + \sqrt{k_1(4+k_1)}}{2}M = 0, \quad (11)$$

also valid for $0 < k_1 < k_{1\_P_c}$.

As evidenced in [5], equations (2)-(11) are valid for the case of a SEPIC or a Ćuk converter with an extra diode at its input port.

B. Case of Full-Wave Rectified Sinusoidal input Voltage and DCM Operation

A SEPIC converter connected to an AC line through a line rectifier is shown in Fig. 2. In order to potentially work as RE, the SEPIC converter must be working in one DCM. Due to the line rectifier, the current passing through input inductor L_1 cannot reverse, leading to a situation similar to the one shown in Fig. 1, but now with a full-wave rectified sinusoidal input voltage. As in the case of the converter given in Fig. 1, three DCMs will be possible in the converter shown in Fig. 2. However, due to the rectified line voltage at the converter input port, all the electrical parameters are synchronously changing with the line angle φ. Therefore, k_1 and k_2, R and M, must be redefined as $k_1(\varphi)$, $k_2(\varphi)$, $r(R,\varphi)$ and $m(M_{\pi/2},\varphi)$, as detailed below:

$$k_1(\varphi) = \frac{2L_1}{r(\varphi)T_s}, \quad (12)$$

$$k_2(\varphi) = \frac{2L_2}{r(\varphi)T_s} = \alpha k_1(\varphi), \quad (13)$$

$$r(\varphi) = \frac{V_o}{i_o(\varphi)}, \quad (14)$$

$$m(M_\pi,\varphi) = \frac{V_o}{v_g(\varphi)} = \frac{V_o}{V_g|sin(\varphi)|} = \frac{M_{\pi/2}}{|sin(\varphi)|}. \quad (15)$$

In this context, $r(\varphi)$ denotes the effective resistance seen by the SEPIC stage preceding the bulk capacitor C_B, and $M_{\pi/2}$ is the value of M at the peak value of the line voltage, i.e., $M_{\pi/2} = V_o/V_g$, V_g being the peak value of the line voltage. Furthermore, to ensure operation in DCM, an appropriate duty cycle d_{DCM} must be chosen. Consequently, the location of P_c given in (2), the voltage conversion ratios (4)-(7), and the equations defining the boundaries between modes (8)-(11) must be adapted to the situation of having full-wave rectified sinusoidal voltage at the input port. In order to do this, M must be replaced with $m(M_{\pi/2},\varphi)$ in the above-mentioned equations. The coordinates of $P_c(\varphi)$ are now:

$$k_{1\_P_c}(M_{\pi/2},\varphi) = \frac{sin^2(\varphi)}{M_{\pi/2}(M_{\pi/2}+|sin(\varphi)|)},$$
$$k_{2\_P_c}(M_{\pi/2},\varphi) = \frac{|sin(\varphi)|}{M_{\pi/2}+|sin(\varphi)|}. \quad (16)$$

As the voltage conversion ratio in each mode is now determined by φ, according to (15), and the values of k_1 and k_2 are related by (13), then equations (4)-(7) allow us to determine the value of k_1 in each DCM. The resulting equations are the following:

- When operating in DCM1, (4) becomes:

$$\frac{M_{\pi/2}}{|sin(\varphi)|} - \frac{d_{DCM}}{\sqrt{\frac{\alpha}{1+\alpha}k_1(\varphi)}} = 0. \quad (17)$$

- When operating in DCM2, (5) becomes:

$$\frac{M_{\pi/2}}{|sin(\varphi)|} - \frac{k_1(\varphi)+\sqrt{k_1(\varphi)(4+k_1(\varphi))}}{2k_1(\varphi)}d_{DCM} = 0. \quad (18)$$

- When operating in DCM3, (6) and (7) become:

$$\frac{M_{\pi/2}}{|sin(\varphi)|} - \frac{A(\varphi)+\sqrt{A(\varphi)^2+16\alpha^2k_1(\varphi)}}{4\alpha k_1(\varphi)}d_{DCM} = 0, \quad (19)$$

where:

$$A(\varphi) = -d_{DCM} + \sqrt{d_{DCM}^2 + 4\alpha k_1(\varphi)}. \quad (20)$$

The definitions of the boundaries between conduction modes in (8)-(11) are now updated as follows:

- From (8), the boundary between CCM and DCM1 becomes:

$$k_2(\varphi) = \frac{k_1(\varphi)sin^2(\varphi)}{(|sin(\varphi)|+M_{\pi/2})^2k_1(\varphi) - sin^2(\varphi)}, \quad (21)$$

which is valid only for $k_1(\varphi) > k_{1\_Pc}(M_{\pi/2},\varphi)$.

- From (9), the boundary between CCM and DCM2 becomes:

$$k_1(\varphi) = \frac{sin^2(\varphi)}{M_{\pi/2}(M_{\pi/2}+|sin(\varphi)|)}, \quad (22)$$

only valid when $k_2(\varphi) > k_{2\_Pc}(M_{\pi/2},\varphi)$.

- From (10), the boundary between DCM1 and DCM3 becomes:

$$k_2(\varphi) = \frac{M_{\pi/2}}{|sin(\varphi)|}k_1(\varphi), \quad (23)$$

valid only for values verifying $0 < k_1(\varphi) < k_{1\_Pc}(M_{\pi/2},\varphi)$.

- From (11), the boundary between DCM2 and DCM3 becomes:

$$k_2(\varphi) = 1 - \frac{-k_1(\varphi)+\sqrt{k_1(\varphi)(4+k_1(\varphi))}}{2|sin(\varphi)|}M_{\pi/2}, \quad (24)$$

which is also valid for $0 < k_1(\varphi) < k_{1\_Pc}(M_{\pi/2},\varphi)$.

The conduction maps obtained after drawing these boundaries in the k_1k_2 plane are shown in Fig. 4 for several values

of φ. In this figure, an example of trajectory has also been drawn, and the converter operating point has been highlighted on this trajectory for each value of φ.

III. The SEPIC and Ćuk Converters as Automatic Power Factor Correctors in Unusual DCMs

A. Approach to Determine the Line Current Waveform

It is very well known that the SEPIC can operate as APFC in the case of being designed to always operate in DCM1 [2]. In order to increase power density, L_1 can be reduced. However, if L_1 is low enough, operation in DCM2 and DCM3 will be reached due to the input rectifier diodes. It leads to the need of computing the line current waveform considering not only DCM1, but also DCM2 and DCM3, in order to evaluate the APFC performance in this scenario.

Now, let us establish a power balance between the converter input and output ports. Firstly, this balance is established for each line angle φ, averaging the electrical quantities over a switching period:

$$v_g(\varphi)i_g(\varphi) = V_o i_o(\varphi), \tag{25}$$

where $i_g(\varphi)$ is the value obtained after averaging the current passing through L_1 over a switching period T_s and $i_o(\varphi)$ is the current injected by the converter into the output RC_B network. From (15) and (25), we can easily obtain:

$$i_g(\varphi) = \frac{M_{\pi/2}}{|sin(\varphi)|} i_o(\varphi). \tag{26}$$

By employing equations (12) and (14), it can be deduced:

$$i_o(\varphi) = \frac{V_o T_s}{2L_1} k_1(\varphi), \tag{27}$$

and, from (26) and (27), we finally obtain:

$$i_g(\varphi) = \frac{M_{\pi/2}}{|sin(\varphi)|} \frac{V_o T_s}{2L_1} k_1(\varphi). \tag{28}$$

From (28), it is evident that the determination of $k_1(\varphi)$ (or $k_2(\varphi)$, given their relationship through α) is essential in order to determine the line current waveform.

The expressions for $k_1(\varphi)$ in each DCM can be derived from (17)-(20).

- DCM1:

$$k_1(\varphi) = \frac{1+\alpha}{\alpha} \Big(\frac{d_{DCM}}{M_{\pi/2}}\Big)^2 sin^2(\varphi). \tag{29}$$

- DCM2:

$$k_1(\varphi) = \frac{d_{DCM}^2}{M_{\pi/2}\big(M_{\pi/2} - d_{DCM}|sin(\varphi)|\big)} sin^2(\varphi). \tag{30}$$

- DCM3: in this case, the implicit function defined by (19) and (20) does not generate a closed-form equation for $k_1(\varphi)$. Consequently, the value of $k_1(\varphi)$ must be obtained by solving (19) and (20) for each value of φ.

As an example, let us analyze $i_g(\varphi)$ in two hypothetical cases:

- The converter always operates in DCM1 during the entire line half-cycle. In this case, from (28), (29) and the definition of $M_{\pi/2}$, we obtain:

$$i_g(\varphi) = \frac{d_{DCM}^2(1+\alpha)T_s}{2\alpha L_1} V_g|sin(\varphi)|. \tag{31}$$

  This result demonstrates that the converter works as an ideal RE in the DCM1. It is the recognized scenario where the converter acts an ideal APFC. As demonstrated in the following sub-section, the converter can be designed to operate always in DCM1 and, therefore, this situation is possible.
- The converter always operates in DCM2 during the entire line half-cycle. In this case, from (28), (30) and the definition of $M_{\pi/2}$, we obtain:

$$i_g(\varphi) = \frac{M_{\pi/2}T_s}{2L_1} \frac{d_{DCM}^2}{\big(M_{\pi/2} - d_{DCM}|sin(\varphi)|\big)} V_g|sin(\varphi)|. \tag{32}$$

  This result demonstrates that the converter does not work as an ideal RE in the DCM2.

As demonstrated in the following sub-section, the converter cannot be designed to operate in DCM2 during the entire line half-cycle and, therefore, this situation is not possible. However, the converter can be designed to operate in DCM2 during a part of the line half-cycle.

B. Determination of $k_1(\varphi)$ Evolution

As explained before, the determination of the evolution of $k_1(\varphi)$ is the key point to determine $i_g(\varphi)$, according to (28). The evolution of $k_1(\varphi)$ in the $k_1(\varphi)k_2(\varphi)$ plane set depends on the position of the operating point P_φ along the trajectory defined by α. In order to allow the converter to work as a RE, the operating point at $\varphi = \pi/2$ and full load must be placed in one of the DCMs. We will call $P_{\pi/2}$ the operating point at $\varphi = \pi/2$ and full load. Its coordinates are $k_1(\pi/2)$ and $k_2(\pi/2)$.

It should be noted that $P_{\pi/2}$ represents the farthest operating point from the origin in the $k_1(\varphi)k_2(\varphi)$ plane. As φ moves away from $\pi/2$, the operating point moves along the trajectory away from $P_{\pi/2}$, until it reaches the origin of the $k_1(\varphi)k_2(\varphi)$ plane when the line voltage crosses zero.

The position of point $P_{\pi/2}$ in map $k_1(\pi/2)k_2(\pi/2)$ is the starting point to analyze the evolution of $k_1(\varphi)$. If we draw a straight line from point P_c to the origin, then this straight line coincides with the boundary between DCM1-DCM3 (see Fig. 4). From (16), the slope of this straight line is:

$$\frac{k_{2\_P_c}(M_{\pi/2}, \frac{\pi}{2})}{k_{1\_P_c}(M_{\pi/2}, \frac{\pi}{2})} = M_{\pi/2}. \tag{33}$$

As the slope of the trajectory is α and $P_{\pi/2}$ must be placed in any of the DCMs, then two possible situations must be taken into consideration. If $P_{\pi/2}$ is placed in DCM1 (which also means $M_{\pi/2} > \alpha$), then the converter will operate as ideal APFC, which is the well-known operation mode. Just on the other hand, if $M_{\pi/2} < \alpha$ (low L_1 approach), then $P_{\pi/2}$ is

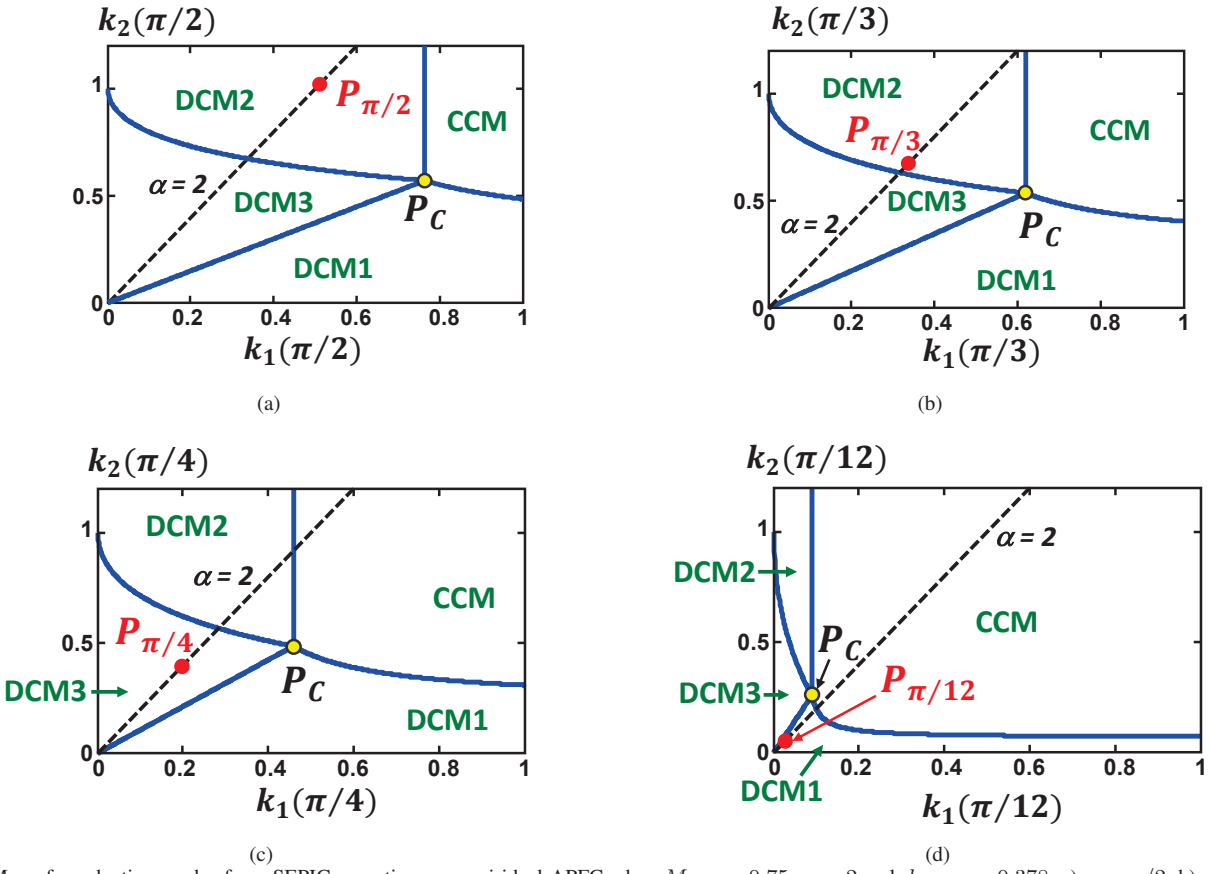

Fig. 4. Map of conduction modes for a SEPIC operating as quasi-ideal APFC when $M_{\pi/2} = 0.75$, $\alpha = 2$ and $d_{DCM} = 0.378$. a) $\varphi = \pi/2$. b) $\varphi = \pi/3$. c) $\varphi = \pi/4$. d) $\varphi = \pi/12$.

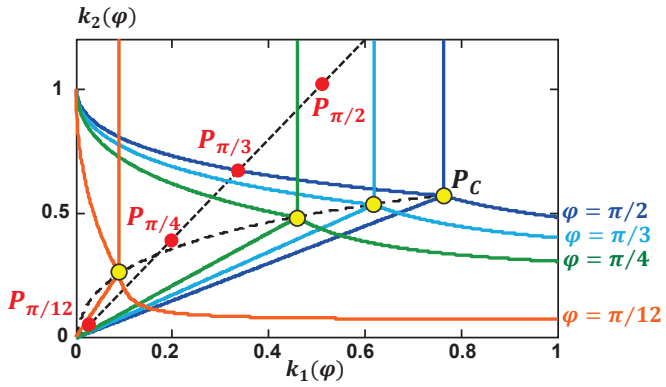

Fig. 5. Conduction map that summarizes the information given in the maps of Fig. 4.

placed either in DCM2 or DCM3 and, consequently, the line waveform does not correspond to an ideal APFC. To properly determine the line waveform, the evolution of $k_1(\varphi)$ must be carefully computed in a line half-cycle, according to (29), (30) and the solution of the implicit equation defined by (19) and (20).

As line angle φ is constantly changing, the boundaries between conduction regions and operating point P_φ (always along the trajectory) are also constantly changing as a function of φ. Consequently, the position of operating point P_φ can be placed in different DCMs, as the example given in Fig. 4 shows. To study the evolution of the boundaries between conduction regions, let us describe the evolution of the straight line that defines the boundary between DCM1-DCM3 when φ changes. From (16), the slope of this straight line is:

$$\frac{k_{2\_P_c}(M_{\pi/2}, \varphi)}{k_{1\_P_c}(M_{\pi/2}, \varphi)} = \frac{M_{\pi/2}}{|sin(\varphi)|}. \tag{34}$$

The set of maps shown in Fig. 4 has been gathered in Fig. 5 in a single map that summarizes the information given in the previous maps. This map also shows the evolution of central point P_c and of the DCM1-DCM3 boundary when φ changes.

As (34) shows, the slope of the DCM1-DCM3 boundary becomes vertical when φ approaches zero. This conclusion is extremely important, because it means that the converter always reaches operation in DCM1 when the line voltage approaches zero, as Fig. 4(d) shows. If the converter has been designed placing $P_{\pi/2}$ in DCM1 (and, therefore, according to $M_{\pi/2} > \alpha$), the converter will remain in DCM1 during the entire line half-period. Just on the other hand, if the converter has been designed according to $M_{\pi/2} < \alpha$, two possible cases arise:

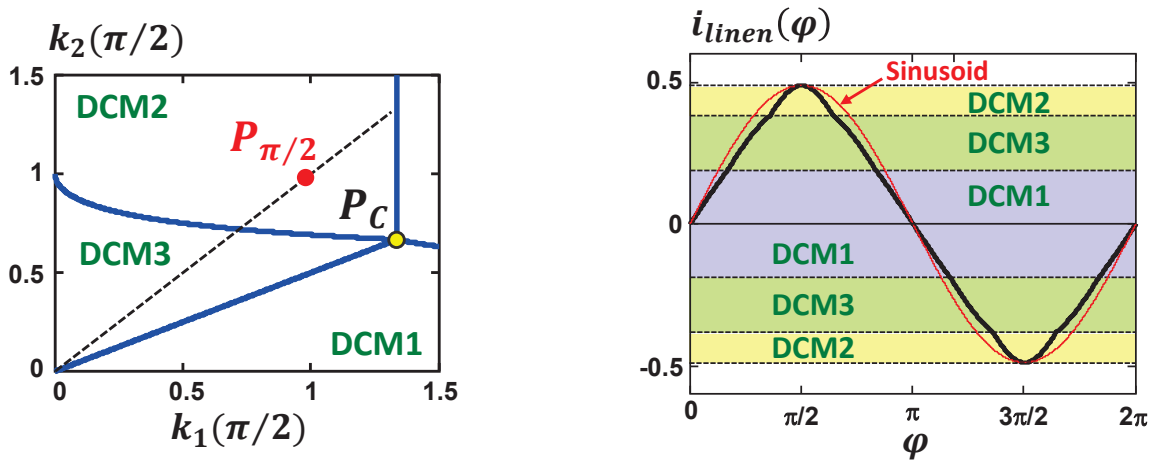

(a) (b)

Fig. 6. Example of design: $M_{\pi/2} = 0.5$, $\alpha = 1$ and $d_{DCM} = 0.307$. a) Position of $P_{\pi/2}$ in the conduction map. b)Normalized line current.

- Case 1: if $P_{\pi/2}$ is located in DCM2, then the operating point progresses from DCM2 to DCM3, and finally reaches DCM1.
- Case 2: if $P_{\pi/2}$ is placed in DCM3, then the operating point evolves from DCM3 to DCM1.

If $P_{\pi/2}$ is placed in DCM2 (Case 1), the value of $k_1(\varphi)$ while the converter remains in this mode is given by (30). As commented before, the evolution of $i_g(\varphi)$ in this mode does not correspond to a sinusoidal evolution. As the angle moves away from $\pi/2$ towards 0, the operating point also moves along the trajectory until it reaches a certain value of φ, labeled as φ_{2-3}, corresponding to leave DCM2 and enter into DCM3. The value of this angle can be computed from (24), (30) and the definition of α, obtaining:

$$\varphi_{2-3} = arcsin\Big(\frac{d_{DCM} - 1 + B}{2\alpha d_{DCM}} M_{\pi/2}\Big), \tag{35}$$

where,

$$B = \sqrt{(1 - d_{DCM})(1 - d_{DCM} + 4\alpha)}. \tag{36}$$

Once the operating point enters into the region corresponding to DCM3, the value of $k_1(\varphi)$ is determined by (19) and (20). However, the operating point always enters into the DCM1 when φ continues decreasing towards 0. When the slope of the straight line that defines the boundary DCM1-DCM3 is steeper than the slope of the trajectory, then the converter starts operating in DCM1. From (34) and the definition of α, we obtain:

$$\varphi_{3-1} = arcsin\Big(\frac{M_{\pi/2}}{\alpha}\Big), \tag{37}$$

where φ_{3-1} is the value of φ corresponding to this boundary. As the converter is operating in DCM1, $k_1(\varphi)$ is calculated again using (29).

In order to prevent the converter from operating in CCM when $\varphi = \pi/2$, the following condition, derived from (3), must be satisfied:

$$d_{DCM} < \frac{M_{\pi/2}}{M_{\pi/2} + 1}. \tag{38}$$

Furthermore, if the objective is to ensure that the converter operates in DCM2 at $\varphi = \pi/2$, the determination of the duty cycle value at the DCM2-DCM3 boundary becomes critical. From (30) and (24), we obtain the value of the duty cycle needed to design the converter just in the above-mentioned boundary:

$$d_{DCM2-3} = \frac{M_{\pi/2}}{2(\alpha - M_{\pi/2})}\Big(\sqrt{(1 - M_{\pi/2}^2) + 4\alpha} - M_{\pi/2} - 1\Big). \tag{39}$$

Therefore, the following inequality must be verified to place $P_{\pi/2}$ in DCM2:

$$d_{DCM2-3} < d_{DCM} < \frac{M_{\pi/2}}{M_{\pi/2} + 1}. \tag{40}$$

On the other hand, $P_{\pi/2}$ is placed in DCM3 if:

$$0 < d_{DCM} < d_{DCM2-3}. \tag{41}$$

As commented before, it should be noted that all these equations can also be applied to the Ćuk converter when used in the same conditions.

C. Design Procedure to Operate in the Unusual DCMs

The input data for the design will be the output voltage and current, V_o and I_o, and the peak value of the line voltage, V_g. Consequently, $M_{\pi/2}$ is an input data, as well.

- The first step in the design procedure is to select the position of $P_{\pi/2}$ in the map corresponding to $M_{\pi/2}$, according to several possible criteria (line distortion, conduction and switching losses, etc.). Once the coordinates of $P_{\pi/2}$ are known, the value of α is fixed. The equation needed to compute the value of d_{DCM} will depend on the region where $P_{\pi/2}$ is placed. Thus, it will be (18) for DCM2 and the set (19) and (20) for DCM3.

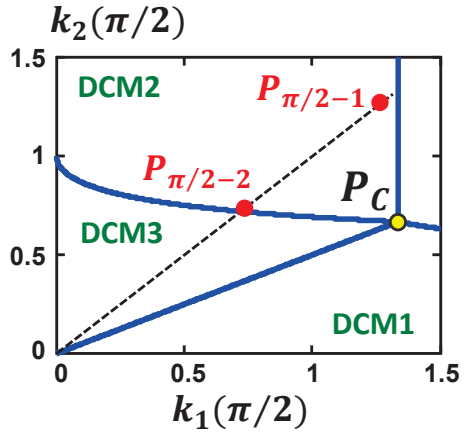

Fig. 7. Design points used for validating the theoretical predictions.

- The second step is to determine the evolution of $k_1(\varphi)$ from $\varphi = 0$ to $\varphi = \pi$ (in fact, to determine the evolution from $\varphi = 0$ to $\varphi = \pi/2$ is enough, due to the waveform symmetry). Afterwards, the average value of $k_1(\varphi)$ must be computed as follows:

$$K_{1avg} = \frac{1}{\pi}\int_o^{\pi} k_1(\varphi)d\varphi. \tag{42}$$

- As the average value of $i_o(\varphi)$ is I_o, (27) allows us to determine L_1 as follows:

$$L_1 = \frac{V_o T_s}{2I_o} K_{1avg}. \tag{43}$$

- Finally, $L_2 = \alpha L_1$.

D. Design Example

A design example is shown in Fig. 6. In this example, $P_{\pi/2}$ is placed in the DCM2. The design values are $M_{\pi/2} = 0.5$, $\alpha = 1$ and $k_1(\pi/2) = k_2(\pi/2) = 0.977$. The value of the duty cycle corresponding to place $P_{\pi/2}$ in this position is obtained from (18), the result being $d_{DCM} = 0.307$. The values of line angles where the conduction mode changes are $\varphi_{2-3} = 64.7°$ and $\varphi_{3-1} = 30°$, obtained from (35), (36) and (37). The equation for $k_1(\varphi)$ is (18) when operating in DCM2, it must be obtained from (19) and (20) in DCM3, and it is (17) in DCM1. Once the evolution of $k_1(\varphi)$ is completely determined, current $i_g(\varphi)$ is directly obtained from (28). Line current waveform $i_{line}(\varphi)$ can be easily built from $i_g(\varphi)$, which is a rectified version of $i_{line}(\varphi)$. A normalized version of $i_{line}(\varphi)$ can be defined as:

$$i_{linen}(\varphi) = \frac{2L_1}{V_o T_s} i_{line}(\varphi). \tag{44}$$

The waveform obtained for this quantity is shown in Fig. 6(b). This figure shows that a low distorted line current waveform can be obtained when the SEPIC converter is designed to operate satisfying $\alpha > M_{\pi/2}$. This is an important conclusion, because this design implies a lower value of inductor L_1 than in the classical design, according to the definition of α. Therefore, quasi-ideal RE behavior can be achieved even if the value of inductor L_1 is similar to the value of inductor L_2.

IV. Validation

The circuit shown in Fig. 2 was implemented to validate the theoretical analysis. The description of the power converter components are as follows: $C = 330$ nF, $C_O = 6.8$ μF, $C_B = 11880$ μF, $L_1 = L_2 = 200$ μH (which means $\alpha = 1$). The study carried out in this prototype evaluates line current waveforms when $P_{\pi/2}$ is placed in two different positions along the trajectory defined by $\alpha = 1$, under the condition of a constant voltage conversion ratio $M_{\pi/2} = 0.5$ ($V_o = 77.8$ V, $V_g = 110\sqrt{2}$ V (50 Hz)). It should be noted that condition $\alpha > M_{\pi/2}$ is satisfied, allowing the converter to operate in multiple DCMs, as previously explained. The analyzed operating points are:

- Point $P_{\pi/2-1}$: $P_{\pi/2}$ is located in DCM2 far from the boundary between this mode and DCM3. This position is achieved with $d = 0.33$ and $R = 73.1$ Ω.
- Point $P_{\pi/2-1}$: $P_{\pi/2}$ is placed in DCM2 nearer to the boundary between this mode and DCM3. This position is attained with $d = 0.282$ and $R = 110$ Ω.

The position of both points in the map of conduction regions corresponding to $\varphi = \pi/2$ is depicted in Fig. 7. The coordinates of $P_{\pi/2-1}$ are $k_1(\pi/2) = k_2(\pi/2) = 1.28$, whereas those of $P_{\pi/2-2}$ are $k_1(\pi/2) = k_2(\pi/2) = 0.73$.

Theoretical, simulated, and experimental line current waveforms are presented in Fig. 8 (results for $P_{\pi/2-1}$), and Fig. 9 (for $P_{\pi/2-2}$). The theoretical line waveforms (in normalized version) were derived by evaluating $k_1(\varphi)$ according to the study described in this paper (Fig. 8(a) and Fig. 9(a)). The waveforms depicted in Fig. 8(b) and Fig. 9(b) were generated using PSIM software, whereas Fig. 8(c) and Fig. 9(c) correspond to the experimental results obtained in the prototype described above. The close agreement between the theoretical predictions, the simulations and the experimental results demonstrates the validity of the theoretical analysis. Trajectory $\alpha = 1$ and voltage conversion ratio $M_{\pi/2} = 0.5$ were conveniently chosen to illustrate that the line current does not exhibit a pure sinusoidal waveform when $P_{\pi/2}$ is on a trajectory that satisfies $\alpha > M_{\pi/2}$. However, the THD measured in the prototype for operating points $P_{\pi/2-1}$ and $P_{\pi/2-2}$ were 10 % and 5.3 % respectively, values that are low enough for most applications. It should be noted that the evolution of the converter following a trajectory that satisfies $\alpha > M_{\pi/2}$ is because the value of L_1 has been chosen lower than the one needed to operate always in DCM1. Therefore, the selection of this type of trajectory leads to a slight increase in THD, but enhances the power density.

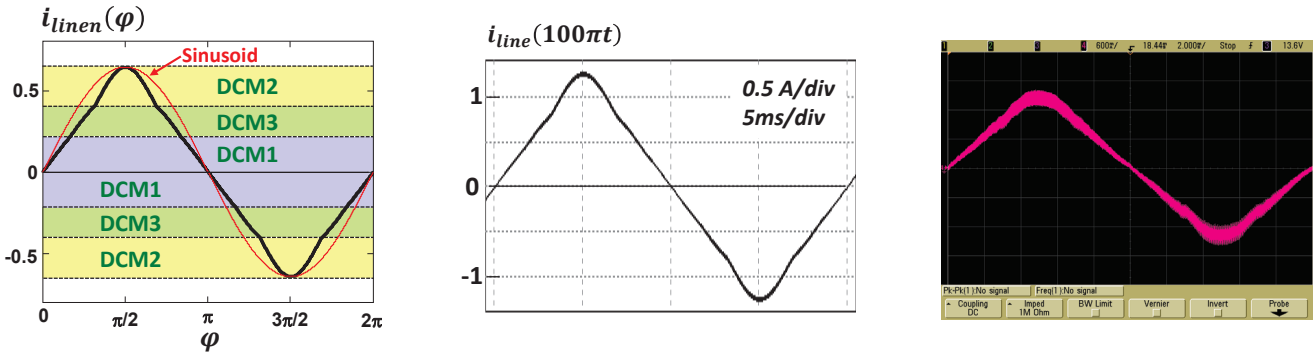

(a) (b) (c)

Fig. 8. Line current waveforms corresponding to design point with $P_{\pi/2-1}$): a) Predicted normalized waveform. b) Simulated waveform. c) Measured waveform in the prototype.

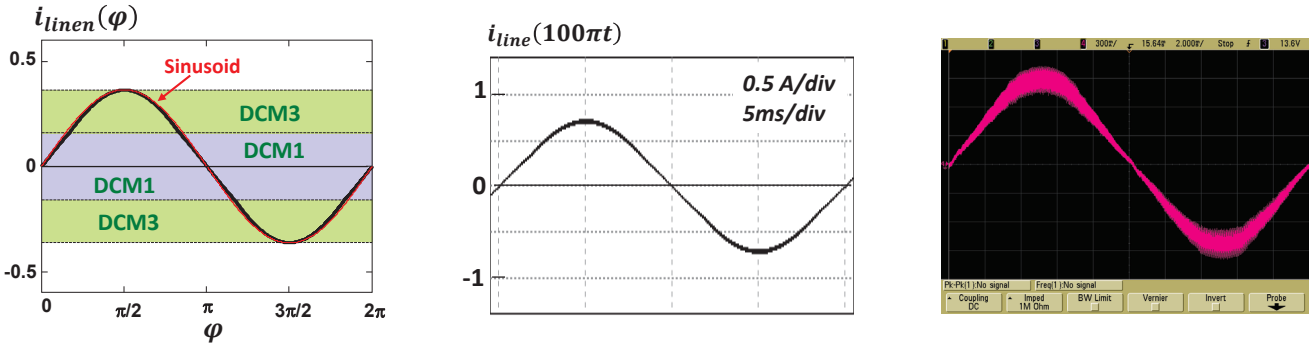

(a) (b) (c)

Fig. 9. Line current waveforms corresponding to design point with $P_{\pi/2-2}$: a) Predicted normalized waveform. b) Simulated waveform. c) Measured waveform in the prototype.

V. Conclusion

This work demonstrates that the line current waveforms of SEPIC and Ćuk APFCs with 3 DCMs can be directly obtained from the evolution of the dimensionless parameter $k_1(\varphi)$ along φ. To obtain this evolution, its value in each DCM must be determined, taking into account that the input voltage corresponds to a full-wave rectified sinusoidal waveform, the duty cycle is maintained constant during a line period and the output voltage is essentially constant. Moreover, the analysis must take into account that the boundaries between conduction modes continuously change with φ. The low THD value obtained when operating in the unusual DCMs (corresponding to low L_1 values) opens the possibility of increasing the converter power density. Finally, the theoretical predictions have been successfully validated through simulation and experimental results.

Acknowledgment

This work was supported in part by the Spanish Government under research projects PID2021-127707OB-C21 and PID2022-136969OB-I00. This work was also supported by the Principado de Asturias Government under project SV-PA-21-AYUD/2021/51931 and by the FEDER funding.

References

[1] R. Erickson, M. Madigan, and S. Singer, "Design of a simple high-power-factor rectifier based on the flyback converter," in *Fifth Annual Proceedings on Applied Power Electronics Conference and Exposition*, 1990, pp. 792–801.

[2] J. Sebastian, J. Uceda, J. A. Cobos, J. Arau, and F. Aldana, "Improving power factor correction in distributed power supply systems using pwm and zcs-qr sepic topologies," in *PESC '91 Record 22nd Annual IEEE Power Electronics Specialists Conference*, 1991, pp. 780–791.

[3] M. Brkovic and S. Cuk, "Input current shaper using cuk converter," in *[Proceedings] Fourteenth International Telecommunications Energy Conference - INTELEC '92*, 1992, pp. 532–539.

[4] J. Sebastian, J. Cobos, J. Lopera, and U. Uceda, "The determination of the boundaries between continuous and discontinuous conduction modes in pwm dc-to-dc converters used as power factor preregulators," *IEEE Transactions on Power Electronics*, vol. 10, no. 5, pp. 574–582, 1995.

[5] D. Murillo-Yarce, C. Restrepo, D. G. Lamar, M. M. Hernando, and J. Sebastián, "Study of multiple discontinuous conduction modes in sepic, ćuk, and zeta converters," *Electronics*, vol. 11, no. 22, 2022. [Online]. Available: https://www.mdpi.com/2079-9292/11/22/3744

[6] D. Murillo-Yarce, C. Restrepo, D. G. Lamar, and J. Sebastián, "A general method to study multiple discontinuous conduction modes in dc-dc converters with one transistor and its application to the versatile buck-boost converter," *IEEE Transactions on Power Electronics*, vol. 37, no. 11, pp. 13 030–13 046, 2022.